

PRODUCED PARTICLE RAPIDITY  
(PSEUDORAPIDITY) DISTRIBUTION  
IN Au–Au AND Pb–Pb COLLISIONS  
AT HIGH ENERGY

FU-HU LIU

Institute of Modern Physics, Shanxi Teachers University  
Linfen, Shanxi 041004, China  
e-mail: liufh@dns.sxtu.edu.cn

(Received July 10, 2000; revised version received November 30, 2000)

The rapidity (pseudorapidity) distribution of produced particles in high-energy nucleus–nucleus collisions are studied by the thermalized cylinder model. In the calculation, two rapidity (pseudorapidity) distribution formulas for an isotropic thermal source are used. The calculated results are compared with the experimental data of Au–Au collisions at 11.5A and 10.8A GeV/c and Pb–Pb collisions at 158A GeV/c. The formula for rapidity (pseudorapidity) agrees well with data on rapidity (pseudorapidity) distribution, whereas approximating rapidity (pseudorapidity) by pseudorapidity (rapidity) leads to discrepancies in the fragmentation regions. The fit parameter  $\Delta y$  representing the rapidity interval over which isotropic sources are distributed seems to be independent on the kinds of concerned produced particles and the centrality cut in the fitted data.

PACS numbers: 25.75.–q, 24.01.Pa

## 1. Introduction

The aims of studying nucleus–nucleus collisions at high energy are to find evidence for the production of Quark–Gluon Plasma (QGP) and to investigate the mechanism of nuclear reactions. The knowledge of produced particle rapidity distribution leads to important constraints on the reactions and is of great importance in order to assess. Generally speaking, the spectator does not contribute directly to the produced particles. The produced particles, *e.g.*  $K^\pm$  and  $\pi^\pm$ , are mainly produced in the participant.

A lot of models have been introduced for heavy ion collisions. For example, FRITIOF [1], VENUS [2], RQMD [3], QGSM [4], HIJING [5], ARC [6], Hydrodynamics [7] and Fireball [8] models, *etc.* Based on the fireball model,

we have developed a thermalized cylinder model [9] and described the rapidity ( $y$ ) or pseudorapidity ( $\eta$ ) distributions of relativistic singly charged particles in high energy nucleus–nucleus collisions [10].

In this paper, the rapidity (pseudorapidity) distributions of produced particles in high-energy nucleus–nucleus collisions are studied by the thermalized cylinder model. The calculated results are compared with the experimental data of Au–Au collisions at  $11.5A$  and  $10.8A$  GeV/ $c$  and Pb–Pb collisions at  $158A$  GeV/ $c$ . In the calculation, two rapidity (pseudorapidity) distribution formulas for an isotropic thermal source are used.

## 2. The model

Let us consider the simplest pictures of the one-dimensional string model [11] and the fireball model [8]. In a high energy nucleon–nucleon collision, a string is formed consisting of two endpoints acting as energy reservoirs and the interior with constant energy per length. Because of the asymmetry of the mechanism, the string will break into many substrings along the direction of the incident beam. The distribution length of substrings will define the width of the rapidity (pseudorapidity) distribution. According to the fireball model, the incident nucleon penetrates through the target nucleon, then a firestreak is formed along the direction of the incident beam. The length of the firestreak will define the width of the rapidity (pseudorapidity) distribution. In high-energy nucleus–nucleus collisions, many strings or firestreaks are formed along the incident direction. Finally, a thermalized cylinder is formed because these strings or firestreaks stack and exchange their momenta in the transverse direction.

In the laboratory reference frame, we assume that the thermalized cylinder formed in nucleus–nucleus collisions is in the rapidity range  $[y_{\min}, y_{\max}]$ . The emission points with the same rapidity,  $y_x$ , in the thermalized cylinder form a cross section (emission source) in the rapidity space. For the thermalized cylinder, the initial extension of the nuclei is not important because of Lorentz-contraction.

Under the assumption that the particles are emitted isotropically in the rest frame of the emission source, we know that the pseudorapidity distribution of the particles produced in the emission plane with rapidity  $y_x$  in the laboratory reference frame is

$$f(\eta, y_x) = \frac{1}{2 \cosh^2(\eta - y_x)}. \quad (1)$$

In final state, the  $\eta$  distribution is contributed by the whole thermalized

cylinder. We have

$$f(\eta) = \frac{1}{y_{\max} - y_{\min}} \int_{y_{\min}}^{y_{\max}} f(\eta, y_x) dy_x. \quad (2)$$

Replacing  $\eta$  by  $y$  in Eq. (2) due to  $\eta \approx y$  at high energy [12], the rapidity distribution can be obtained. Generally speaking, the variables  $\eta$  and  $y$  always satisfy the inequality:  $|\eta| \geq |y|$ , where the equality obtains if and only if for massless particles. For a particle with high energy, if its rest mass can be neglected comparing with its energy, we have  $\eta \approx y$ .

Let  $y_C$  denote the mid-rapidity of produced particles. We have

$$\begin{aligned} y_{\min} &= y_C - \Delta y, \\ y_{\max} &= y_C + \Delta y, \end{aligned} \quad (3)$$

where  $\Delta y$  is the rapidity shift.

The emission source with rapidity  $y_x$  can be regarded as an isotropic thermal source. According to the isotropic thermal model [13], in the center-of-mass frame of the source, the probability ( $P$ ) distribution in momentum ( $p$ ) space can be assumed as

$$\frac{d^3 P}{d^3 p} = A \exp\left(-\frac{E}{T}\right), \quad (5)$$

where  $A$  is a normalization constant,  $E$  is the energy, and  $T$  is the temperature. Expressed in terms of rapidity and transverse mass, we have

$$\frac{d^2 P}{dm_t dy} = A' m_t^2 \cosh(y - y_x) \exp\left[-\frac{m_t}{T} \cosh(y - y_x)\right], \quad (6)$$

where  $A'$  is a normalization constant,  $m_t = \sqrt{m^2 + p_t^2}$  is the transverse mass, and  $m$  and  $p_t$  are the mass and the transverse momentum, respectively. Performing the integral over  $m_t$ , we find

$$\frac{dP}{dy} = C e^{-\alpha} \left(1 + \frac{2}{\alpha} + \frac{2}{\alpha^2}\right), \quad (7)$$

where  $C$  is a normalization constant, and

$$\alpha = \frac{m}{T} \cosh(y - y_x). \quad (8)$$

In final state, the  $y$  distribution is contributed by the whole thermalized cylinder. We have

$$F(y) = \frac{1}{y_{\max} - y_{\min}} \int_{y_{\min}}^{y_{\max}} \frac{dP}{dy} dy_x. \quad (9)$$

Both Eqs. (2) and (9) can describe the experimental  $\eta$  or  $y$  distributions. Generally speaking, Eq. (2) describes the  $\eta$  distribution and gives approximately a description of the  $y$  distribution. While Eq. (9) describes the  $y$  distribution, and gives approximately a description of the  $\eta$  distribution. If  $T \gg m$ , the leading term in Eq. (7) is then of order  $\alpha^{-2}$ , we have

$$\frac{dP}{dy} \approx \frac{1}{2 \cosh^2(y - y_x)}, \quad (10)$$

and

$$F(y) \approx f(\eta). \quad (11)$$

### 3. Comparison with experimental data

Fig. 1 presents the rapidity distributions of  $K^+$  and  $K^-$  produced in central (4% geometry cross-section  $\sigma_{\text{geo}}$ ) Au–Au collisions at 11.5A GeV/c in the transverse momentum region  $p_t < 30$  MeV/c. The black circles and squares are the experimental  $K^+$  and  $K^-$  invariant multiplicity  $[(1/2\pi p_t)d^2N/dp_t dy]$  distributions respectively [14]. The white circles and squares are reflected about midrapidity ( $y_C = 1.60$ ). The solid curves are our calculated results by Eq. (2). In the calculation, we take  $\Delta y = 0.50$ .

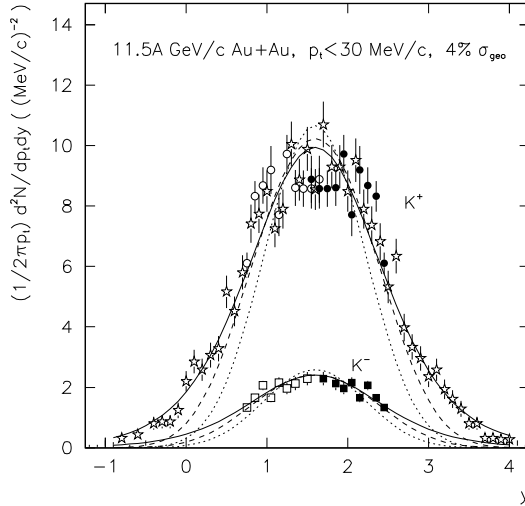


Fig. 1. Rapidity distributions of  $K^+$  and  $K^-$  produced in central Au–Au collisions at 11.5A GeV/c in the transverse momentum region  $p_t < 30$  MeV/c. The black circles and squares are the experimental  $K^+$  and  $K^-$  invariant multiplicity distributions respectively [14], and the white circles and squares are reflected about midrapidity. The stars are our simulated results for  $K^+$  by the Monte Carlo method. The solid curves are our calculated results by Eq. (2), while the dotted and dashed curves are our calculated results by Eq. (9).

The calculated results are scaled to the experimental data in the central rapidity region. Using the same  $\Delta y$  and taking  $T = 180$  MeV, the calculated results of Eq. (9) are shown in the figure by the dotted curves. We see that Eq. (9) gives a narrow distribution. Increasing  $\Delta y$  to 0.80, the calculated

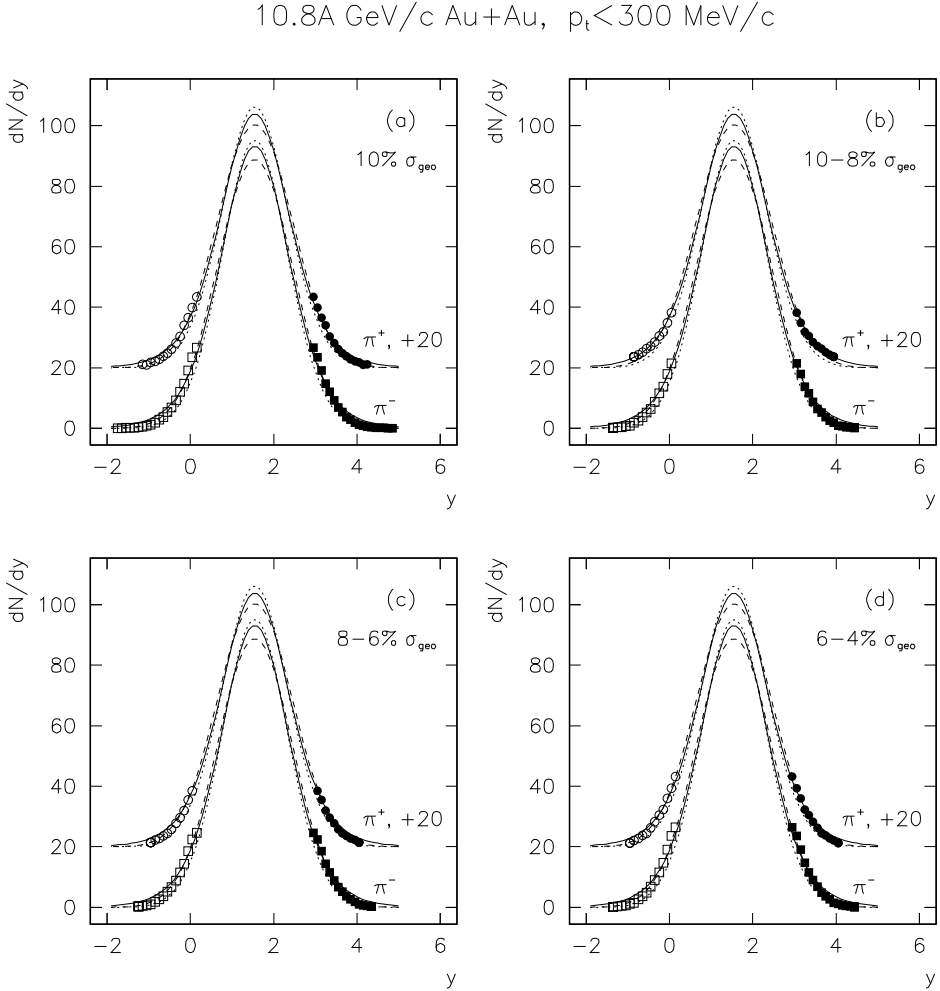


Fig. 2. Rapidity distributions of  $\pi^+$  and  $\pi^-$  produced in different centralities in Au–Au collisions at 10.8A GeV/c in the transverse momentum region  $p_t < 300$  MeV/c. The black circles (scaled by plus 20 for clarity) and squares are the experimental  $\pi^+$  and  $\pi^-$  rapidity distributions respectively [16], and the white circles and squares are reflected about midrapidity. The solid curves are our calculated results by Eq. (2), while the dotted and dashed curves are our calculated results by Eq. (9).

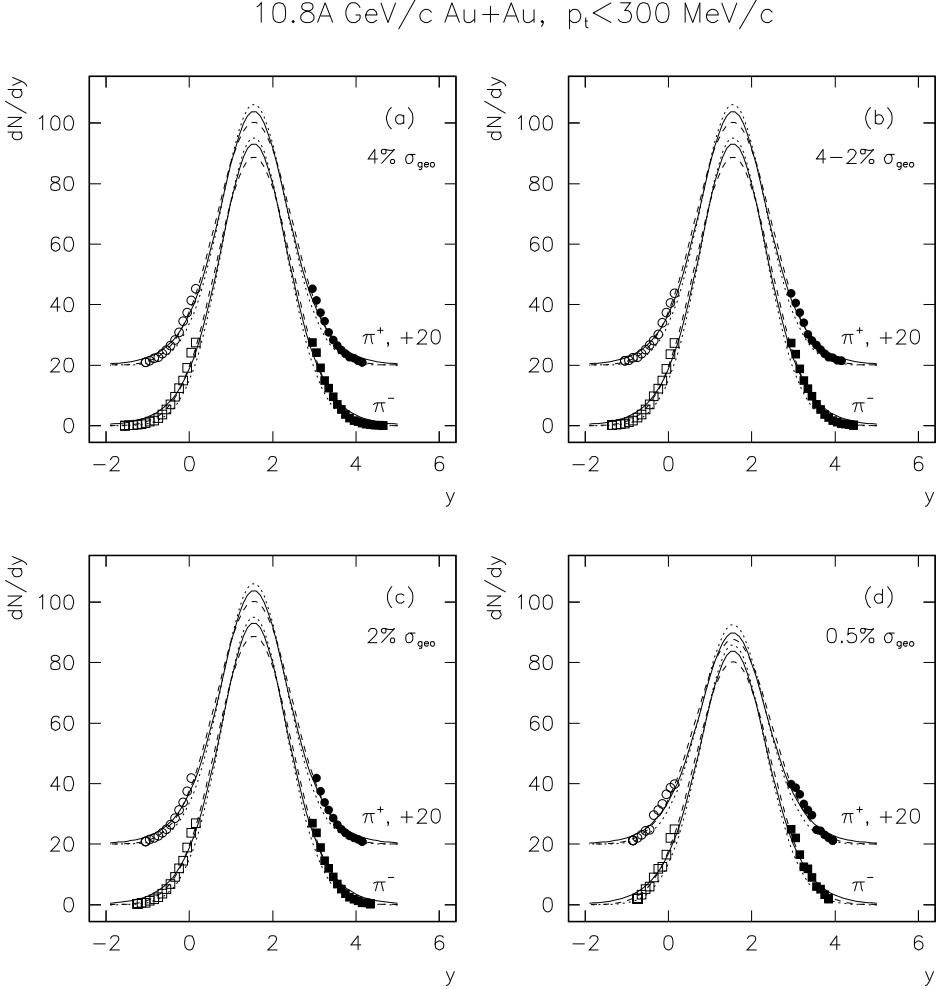


Fig. 3. As for Fig. 2, but showing the results in other centralities.

results of Eq. (9) are given in the figure by the dashed curves. The results of Eq. (9) with  $\Delta y = 0.80$  are close to those of Eq. (2) with  $\Delta y = 0.50$  in the central rapidity region. It is known that Eq. (1) is close to a Gaussian with the standard deviation  $\sigma \approx 0.91$  [15], and Eq. (7) resembles a Gaussian with  $\sigma \approx 0.71$  near its peak at very high temperature [13]. Instead of Eqs. (2) and (9), we use a Gaussian to simulate the rapidity distribution. The stars in Fig. 1 are our Monte Carlo simulated results for  $K^+$  with  $\sigma = 0.82$  and  $\Delta y = 0.50$ . The simulated particle number is 4000. One can see that, in the central rapidity region, the simulated results describe the mean trend and the fluctuation of  $K^+$  rapidity distribution. In Fig. 1, the experimental data

in the projectile and target fragmentation regions (high and low rapidity regions) are not available. Eq. (2) with  $\Delta y = 0.50$  gives a good description, while Eq. (9) with  $\Delta y = 0.80$  and  $T = 180$  MeV gives an acceptable description for the available experimental data.

Figures 2 and 3 present the rapidity distributions of  $\pi^+$  and  $\pi^-$  produced in different centralities in Au–Au collisions at 10.8A GeV/c in the transverse momentum region  $p_t < 300$  MeV/c. The centralities are shown in the figures. The black circles (scaled by plus 20 for clarity) and squares are the experi-

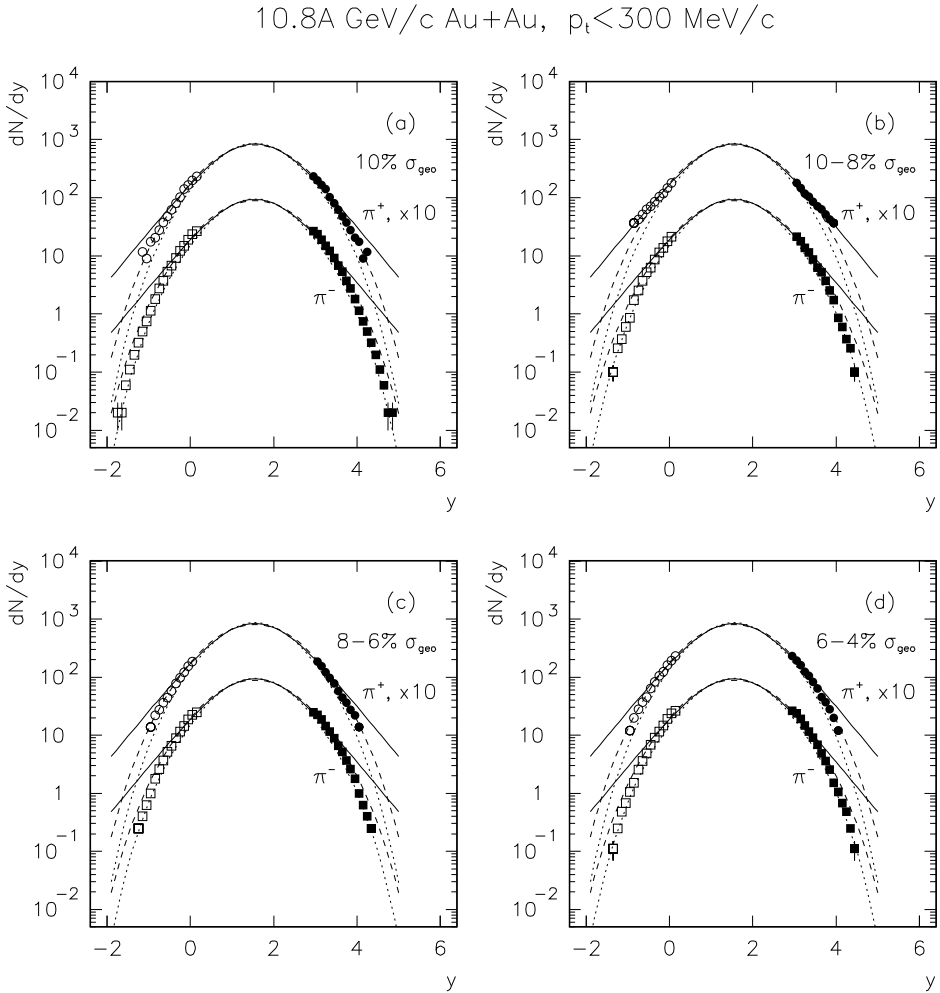


Fig. 4. As for Fig. 2, but the results are given logarithmically and the  $\pi^+$  data are scaled by times 10 for clarity.

mental  $\pi^+$  and  $\pi^-$  rapidity distribution respectively [16]. The white circles and squares are reflected about midrapidity ( $y_C = 1.55$ ). The solid curves are our calculated results by Eq. (2) with  $\Delta y = 0.50$ . The calculated results are scaled to the experimental data in the projectile and target fragmentation regions. Using the same  $\Delta y$  and taking  $T = 180$  MeV, the calculated results of Eq. (9) are shown in the figures by the dotted curves. Increasing  $\Delta y$  to 0.80, the calculated results of Eq. (9) are given in the figures by the dashed curves. One can see that, in the projectile and target fragmentation regions, the calculated results seem to describe the experimental data.

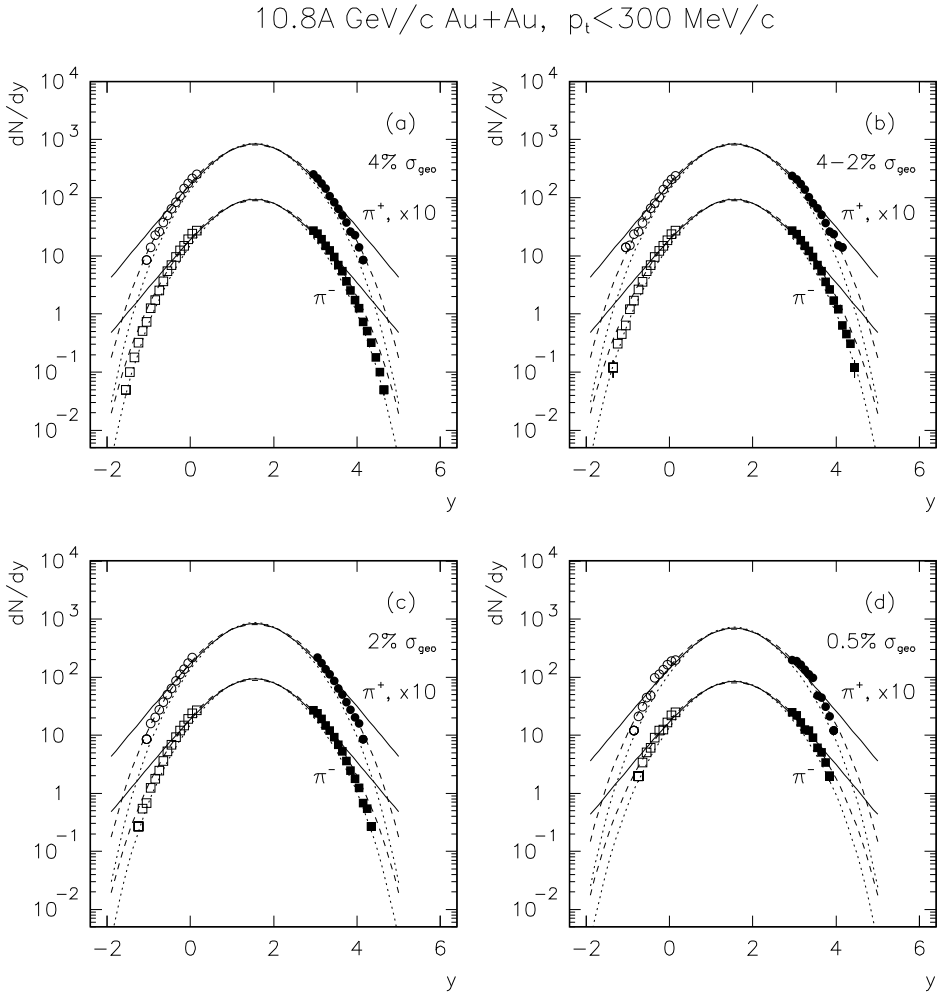


Fig. 5. As for Fig. 3, but the results are given logarithmically and the  $\pi^+$  data are scaled by times 10 for clarity.

Because both the experimental data and the calculated results are very small in the fragmentation regions in Figs. 2 and 3, we redraw them logarithmically in Figs. 4 and 5 respectively. In the figures,  $\pi^+$  data are scaled by times 10 for clarity. It can be seen that Eq. (2) does not describe the rapidity distribution in the tail part except  $\pi^+$  data in Fig. 4(b). Equation (9) with  $\Delta y = 0.50$  and  $T = 180$  MeV gives a good fitting to the  $\pi^-$  data, while a good fitting to the  $\pi^+$  data needs to increase  $\Delta y$  to 0.80.

The pseudorapidity distribution of produced particles in central Pb–Pb collisions at 158A GeV/c is given in Fig. 6(a). The circles are the experimental data [17]. The solid and dotted curves are our calculated results by Eq. (2) with  $\Delta y = 2.60$  and Eq. (9) with  $\Delta y = 2.60$  and  $T = 220$  MeV. The logarithmic distribution is given in Fig. 6(b). We can see that Eq. (2) gives a good description of the data, while Eq. (9) does not fit the tail part of the experimental pseudorapidity distribution. It is difficult to fit the data by increasing  $\Delta y$  in Eq. (9) due to that the calculated distribution shape does not satisfy the data.

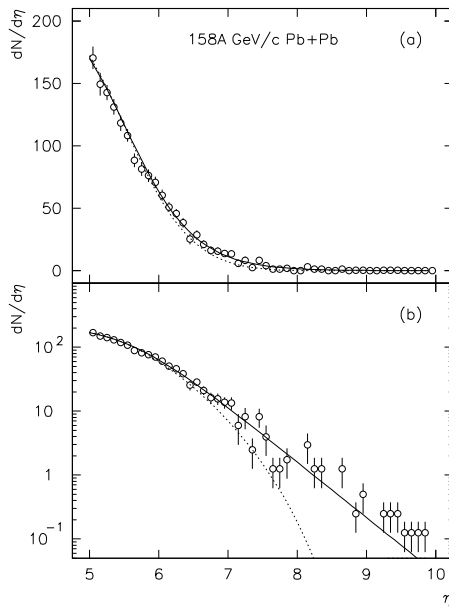


Fig. 6. (a) Pseudorapidity distribution of produced particles in central Pb–Pb collisions at 158A GeV. The circles are the experimental data [17]. The solid and dotted curves are our calculated results by Eqs. (2) and (9) respectively. (b) As for Fig. 6(a), but the results are given logarithmically.

#### 4. Conclusions and discussions

From the above figures, in the fragmentation region, one can see that Eq. (2) gives a good description of the pseudorapidity distribution, while Eq. (9) gives a good description of the rapidity distribution. In the central region, both Eqs. (2) and (9) describe the experimental data. The length ( $2\Delta y$ ) of the thermalized cylinder formed in nucleus–nucleus collisions at a given energy does not depend on the colliding centrality.

We would like to emphasize that the quoted data are not available in the whole region of rapidity (pseudorapidity) distributions. The comparison of formulae and data in Figs. 1–6 is purely qualitative. The quoted parameter values which give a good fitting to the data are just rough guesses.

In Au–Au collisions at  $11.5A$  and  $10.8A$  GeV/ $c$ , we have used the same  $\Delta y$  and the same  $T$  for different particles. This renders that the concerned particles are produced in the same thermalized cylinder. In Pb–Pb collisions at  $158A$  GeV/ $c$ , the values of  $\Delta y$  and  $T$  are greater than those in Au–Au collisions at  $11.5A$  and  $10.8A$  GeV/ $c$ . This renders that the length and the excitation degree of the thermalized cylinder formed in nucleus–nucleus collisions at high energy are greater than those at low energy.

We have used the same  $\Delta y$  and the same  $T$  for different centralities in Au–Au collisions at  $11.5A$  and  $10.8A$  GeV/ $c$ . The independences of  $\Delta y$  and  $T$  on centrality show that the thermalized cylinder formed in nucleus–nucleus collisions is an uniform superposition of strings or firestreaks formed in nucleon–nucleon collisions at the same energy per nucleon. The length and the excitation degree of the thermalized cylinder do not depend on the number of participant nucleons.

Different  $\Delta y$  have been used in Eqs. (2) and (9) for Au–Au collisions at the concerned energies. The value of  $\Delta y$  for Eq. (2) is greater than that for Eq. (9) due to that Eq. (1) has a wide distribution and Eq. (7) has a narrow distribution. The value of  $\Delta y$  is a reflection of the length of the thermalized cylinder.

The thermalized cylinder model is successful in nuclear collisions with a fixed target in the present energy region. We are interested to test the model by the experimental data at the Relativistic Heavy Ion Collider (RHIC) and the Large Hadron Collider (LHC) soon.

For hadronic multiparticle production in  $e^+e^-$  annihilation,  $pp$  collision and  $\pi^+p$  interaction, our previous work [18] based on thermal model show that the particles are isotropically emitted in the local source and the three components of momentum can be regarded as Gaussian type having the same width. This is in agreement with the case in the thermalized cylinder model. The two-source emission picture for nuclear fragments [19] is also in agreement with the present work. We are interested to develop a multisource

ideal gas model to describe the produced particles and nuclear fragments in high-energy collisions with a consistent consideration in the near future.

This work was finished at the Cyclotron Institute of Texas A&M University and supported by the China Scholarship Council. The author's work was also supported by the Shanxi Provincial Foundation for Returned Overseas Scholars, Shanxi Provincial Foundation for Leading Specialists in Science, and Shanxi Provincial Science Foundation for Young Specialists.

## REFERENCES

- [1] G. Gustafson, *Nucl. Phys.* **A566**, 233c (1994), and references therein.
- [2] K. Werner, *Nucl. Phys.* **A566**, 477c (1994), and references therein.
- [3] H. Sorge, H. Stöcker, W. Greiner, *Nucl. Phys.* **A498**, 567c (1989); H. Sorge *et al.*, *Nucl. Phys.* **A525**, 95c (1991); A. Jahns *et al.*, *Z. Phys.* **A341**, 243 (1992); A. Jahns *et al.*, *Nucl. Phys.* **A566**, 483c (1994).
- [4] L.V. Bravina *et al.*, *Nucl. Phys.* **A566**, 461c (1994), and references therein.
- [5] X.N. Wang, *Phys. Rev.* **D43**, 104 (1991); X.N. Wang, M. Gyulassy, *Phys. Rev.* **D44**, 3501 (1991); X.N. Wang, M. Gyulassy, *Phys. Rev. Lett.* **68**, 1480 (1992).
- [6] Y. Pang, T.J. Schlagel, S.H. Kahana, *Nucl. Phys.* **A544**, 435c (1992); Y. Pang, T.J. Schlagel, S.H. Kahana, *Phys. Rev. Lett.* **68**, 2743 (1992); T.J. Schlagel, Y. Pang, S.H. Kahana, *Phys. Rev. Lett.* **69**, 3290 (1992); S.H. Kahana, T.J. Schlagel, Y. Pang, *Nucl. Phys.* **A566**, 465c (1994).
- [7] R.B. Clare, D. Strottman, *Phys. Rep.* **141**, 177 (1986); B.M. Waldhauser *et al.*, *Z. Phys.* **C43**, 411 (1989); M. Hofmann *et al.*, *Nucl. Phys.* **A566**, 15c (1994); U. Ornik, R.M. Weiner, G. Wilk, *Nucl. Phys.* **A566**, 469c (1994).
- [8] W.Y. Chang, *Acta Phys. Sin.* **17**, 271 (1961), and references therein; G.D. Westfall *et al.*, *Phys. Rev. Lett.* **37**, 1202 (1976).
- [9] F.H. Liu, Yu.A. Panebratsev, *Nucl. Phys.* **A641**, 379 (1998); F.H. Liu, Yu.A. Panebratsev, *Phys. Rev.* **C59**, 1193 (1999); F.H. Liu, Yu.A. Panebratsev, *Phys. Rev.* **C59**, 1798 (1999); F.H. Liu, *Acta Phys. Sin.* (Overseas Edition) **7**, 321 (1998); F.H. Liu, *Chin. J. Phys.* **38**, 42 (2000); F.H. Liu, *Nuovo Cim.* **A112**, 1167 (1999); F.H. Liu, Yu.A. Panebratsev, *Can. J. Phys.* **77**, 313 (1999).
- [10] M.I. Adamovich *et al.*, (EMU01 Collaboration), *Z. Phys.* **C56**, 509 (1992); T.H. Burnett *et al.*, *Phys. Rev. Lett.* **50**, 2062 (1983); R. Holyński, *Nucl. Phys.* **A566**, 191c (1994); P. Deines-Jones *et al.*, *Phys. Rev.* **C53**, 3044 (1996); E. Stenlund *et al.*, (EMU01 Collaboration), Proceedings of Quark Matter'95: Abstracts of Contributed Papers, Monterey, California, USA, Jan. 9-13, 1995, p. 215.
- [11] K. Werner, *Phys. Rep.* **232**, 87 (1995).
- [12] M.I. Adamovich *et al.*, (EMU01 Collaboration), *Nucl. Phys.* **A593**, 535 (1995).

- [13] J. Dee, Ph.D thesis, State University of New York at Stony Brook, USA, May 1995.
- [14] Y. Kwon, Ph.D thesis, State University of New York at Stony Brook, USA, May 1997.
- [15] M.I. Adamovich *et al.*, (EMU01 Collaboration), *Phys. Lett.* **B352**, 472 (1995).
- [16] T.W. Piazza, Ph.D thesis, State University of New York at Stony Brook, USA, May 1997.
- [17] P. Deines-Jones *et al.*, *Phys. Rev.* **C62**, 014903 (2000).
- [18] F.H. Liu, Yu.A. Panebratsev, *Nuovo Cim.* **A111**, 1213 (1998); F.H. Liu, *Phys. Rev.* **D62**, 074002 (2000).
- [19] F.H. Liu, Yu.A. Panebratsev, *Nuovo Cim.* **A111**, 1219 (1998); F.H. Liu, Yu.A. Panebratsev, *Phys. Rev.* **C59**, 941 (1999); F.H. Liu, *Phys. Rev.* **C62**, 024613 (2000); F.H. Liu, *Chin. J. Phys.* **38**, 1063 (2000).